Geochronological and Petrological Constraints for Tectonic Evolution of the Central Greater Himalayan Sequence in the Kharta Area, Southern Tibet

Yan Liu, Wolfgang Siebel,[1] *Hans-Joachim Massonne,*[2] *and Xuchang Xiao*[3]

Institute of Geology, Chinese Academy of Geological Sciences, Beijing 100037, China, and State Key Laboratory of Geological Processes and Mineral Resources, China University of Geosciences, Beijing 100083, China (e-mail: yanliu0315@yahoo.com.cn)

ABSTRACT

Within the Kharta area, east of Mount Qomolangma (Everest), garnet sillimanite gneisses and granites including mafic lenses that form the Greater Himalayan Sequence (GHS) were displaced beneath the North Col Formation by the lower South Tibetan Fault (LSTF) and above the Lesser Himalayan Sequence by the Main Central Thrust (MCT). Zircons from mafic lenses, probably former dikes, were dated by thermal ionization mass spectrometry to yield discordant U-Pb results. One sample gave a discordia line with an upper intercept age of 971 Ma, suggesting a late Proterozoic age for emplacement of the dike. Zircon SHRIMP analyses show that the garnet sillimanite gneisses and granites were derived mainly from early Paleozoic rocks produced by high-temperature metamorphism and/or partial melting of Neoproterozoic (meta)sedimentary rocks. These crystalline rocks were buried beneath southern Tibet and experienced metamorphic conditions of 750°–800°C and 14 kbar at 33 ± 2 Ma. After exhumation they were transformed to low-pressure rocks at 23 ± 2 Ma. Structural analyses have revealed that further exhumation of the GHS is attributed to the LSTF and MCT faults beginning at 12–13 Ma, according to monazite U-Th-Pb dating. Finally, these rocks underwent north-south-trending folding at shallow depths after 12 Ma.

Online enhancements: appendix tables.

Introduction

The Himalaya and Tibetan Plateaus are the result of continent-continent (Asia-India) collision. The corresponding collisional events started with subduction of the northernmost Indian plate around 50 Ma (O'Brien et al. 2001; Kaneko et al. 2003; Sachan et al. 2004; Leech et al. 2005). Witnesses of these early subduction-related events are rare eclogites in the western and central Himalayas (see, e.g., Massonne and O'Brien 2003). High-grade metamorphic rocks of crustal origin are also exposed in the Greater Himalayan Sequence (GHS) bounded by the Main Central Thrust (MCT) system along its base and predominantly normal-sense structures of the South Tibetan Fault (STF) system along the top. Knowing more about the activity of the STF and MCT systems—for instance, their timing—will improve our understanding of the collision of India and Asia and the tectonic evolution of both the Himalaya and Tibetan plateaus.

Earlier work suggested that the MCT and STF were active together at early Miocene times (e.g., Hodges et al. 1996). Recent work has shown that both STF and MCT have a long, complex history of activity (e.g., Hodges 2000). Our study contributes to solve the corresponding problem. For that reason, the Kharta area situated more or less in the middle of the Himalayan range (figs. 1, 2*a*), east of Mount Qomolangma (Everest), was investigated in detail. This area is a key location for the tectonic interpretation of the Himalayan structural units linking the eastern and western Himalayas. This article reports new structural, geochemical, and

Manuscript received March 23, 2006; accepted November 13, 2006.

[1] Department of Geosciences, Universität Tübingen, 72074 Tübingen, Germany.

[2] Institut für Mineralogie und Kristallchemie, Universität Stuttgart, 70174 Stuttgart, Germany.

[3] Institute of Geology, Chinese Academy of Geological Sciences, Beijing 100037, China.

[The Journal of Geology, 2007, volume 115, p. 215–230] 0022-1376/2007/11502-0008$15.00

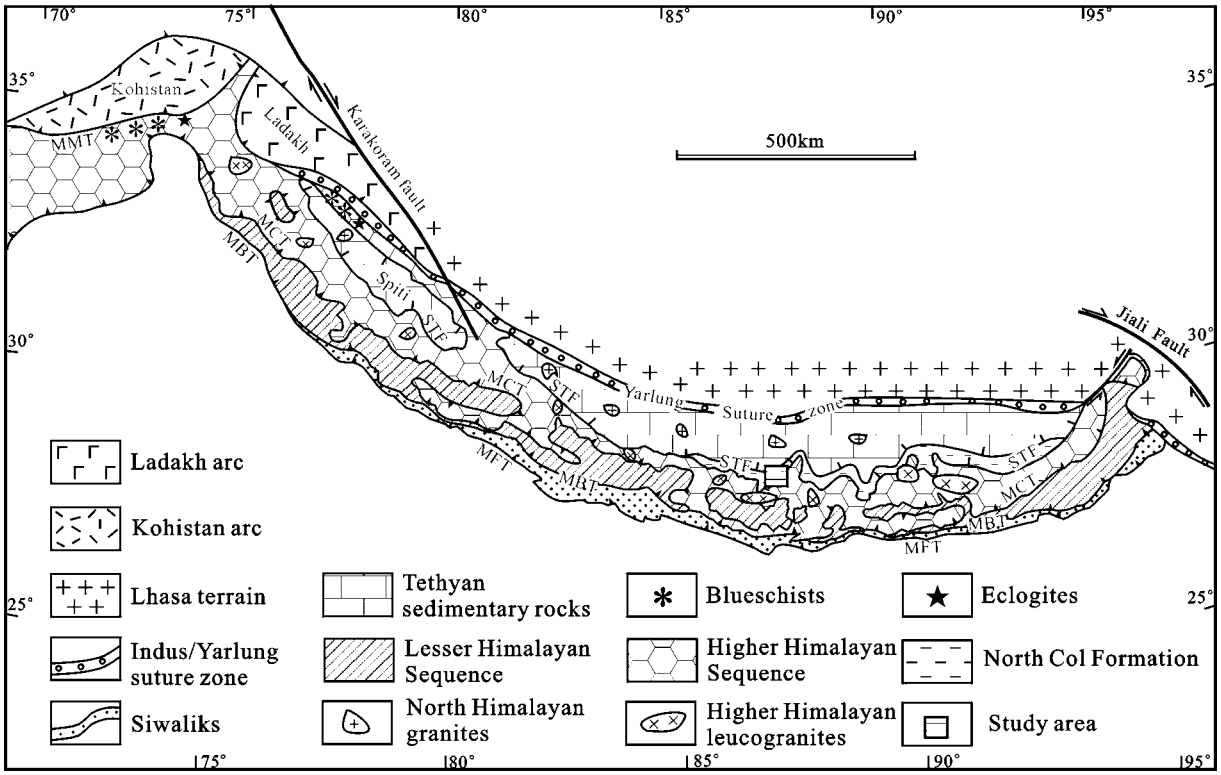

Figure 1. Geological sketch map of the Himalayas, after Chinese scientific mountaineering expeditions to the Mount Jolmo Lungma (1974), Yin and Guo (1978), Wei et al. (1989), Liu et al. (1990), Burchfiel et al. (1992), O'Brien et al. (2001), Searle et al. (2003), and our own observations. *STF* = South Tibetan Fault system; *MCT* = Main Central Thrust system; *MBT* = Main Boundary Thrust system; *MFT* = Main Frontal Thrust system; *MMT* = Main Mantle Thrust system.

geochronological data from the north-trending Kharta valley, which set further constraints on the tectonic evolution of the central GHS.

Geologic Setting

Within the central Himalayas, the metamorphic grade in the GHS first increases in its lower part, which consists of large portions of biotite muscovite gneisses, and then decreases from the middle to the upper part, toward the STF (e.g., Hodges 2000). The major rock types in the middle part of the GHS are garnet sillimanite gneisses marked by sillimanite + K-feldspar and upper-amphibolite facies calc-silicate gneisses (e.g., Borghi et al. 2003). Deformed and undeformed Miocene leucogranites are widespread in the GHS, especially in the upper part, whereas the Lesser Himalayan Sequence (LHS) includes nonfossiliferous lower greenschist to amphibolite facies clastic metasedimentary units (e.g., Hodges 2000). The predominant rock types are impure quartzites, phyllites, schists, paraamphibolite, augen gneisses, and sillimanite biotite muscovite gneisses. Recent Nd isotopic studies indicate that the GHS have slightly higher $^{143}Nd/^{144}Nd$ ratios compared with the LHS ratios, and their $\varepsilon Nd(0)$ values vary from -10 to -19, with a peak at about -15, whereas the $\varepsilon Nd(0)$ values of the LHS are in the range of -23 to -28 (Parrish and Hodges 1996; Whittington et al. 1999; Ahmad et al. 2000; Robinson et al. 2001).

The Kharta area is dominated by the north-northeast-trending Arun anticlinal dome (e.g., Wang and Zheng 1979). There are two different interpretations of the components of this dome. One is that it belongs to the GHS (e.g., Chinese Academy of Sciences 1962, 1974, 1979). Alternatively, the Arun anticlinal dome is interpreted as part of the LHS (Lombardo and Rolfo 2000). In this model, the overprinted eclogites described by Lombardo and Rolfo (2000) to the east of Kharta were regarded as belonging to the LHS. Both interpretations, however, lack solid petrological or isotopic evidence.

Our field investigations revealed that the central

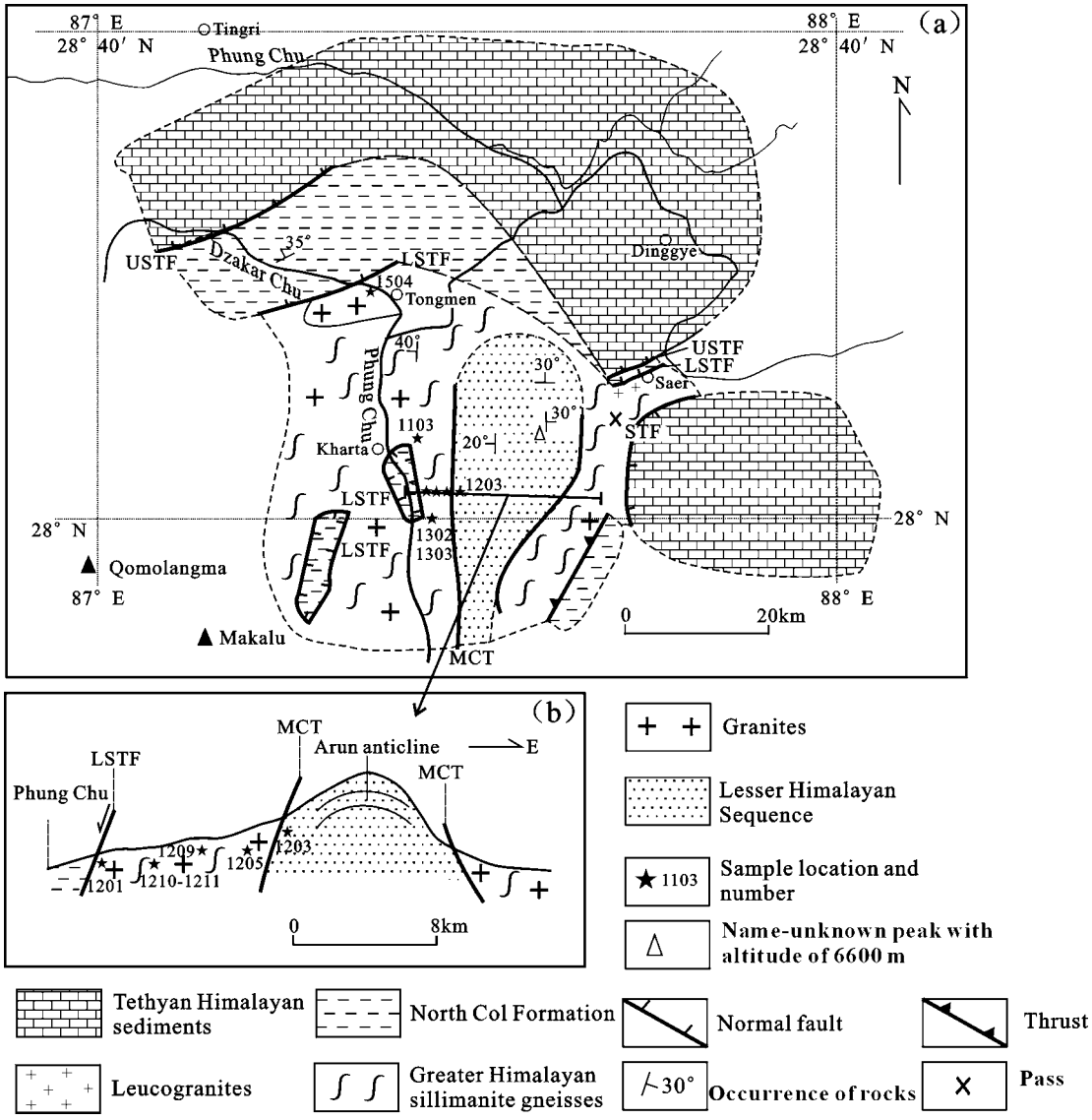

Figure 2. *a*, Geological sketch map of the Kharta area, after Chinese scientific mountaineering expeditions to the Mount Jolmo Lungma (1974, 1979), Yin and Guo (1978), Wei et al. (1989), Searle et al. (2003), and our own observations. *b*, Geological section; for location, see *a*.

parts of the north-northeast-trending Arun anticline are made up of amphibolite facies rocks, including sillimanite gneisses, amphibolites, and calc-silicate rocks. These rocks underwent strong deformation that resulted in mylonites. The dominant schistosity of these rocks strikes north-northeast. To the eastern and western sides of the Arun anticline, the amphibolite facies rocks are separated from garnet sillimanite gneisses, migmatites, and granitoids with mafic lenses in the hanging wall by a high-angle fault (fig. 2*a*). On the western side, this fault, situated about 7 km east of the Phung Chu valley, is dipping to the west (fig. 2). Within the footwall of this fault, the north-northeast-trending stretching lineation, consisting of sillimanite and biotite, was cut by an east-west-trending and west-dipping brittle broken zone, indicating that this fault is a normal fault. On the eastern side, southwest of Saer, this fault corresponds to the east-dipping high-angle fault mapped by Burchfiel et al. (1992) and Hodges et al. (1994; fig. 3).

On the western side of the Arun anticline, the garnet sillimanite gneisses and granites are cut by a north-south-trending normal fault with a width of about 100 m and separated from the North Col Formation in the hanging wall (fig. 2*a*). About 22

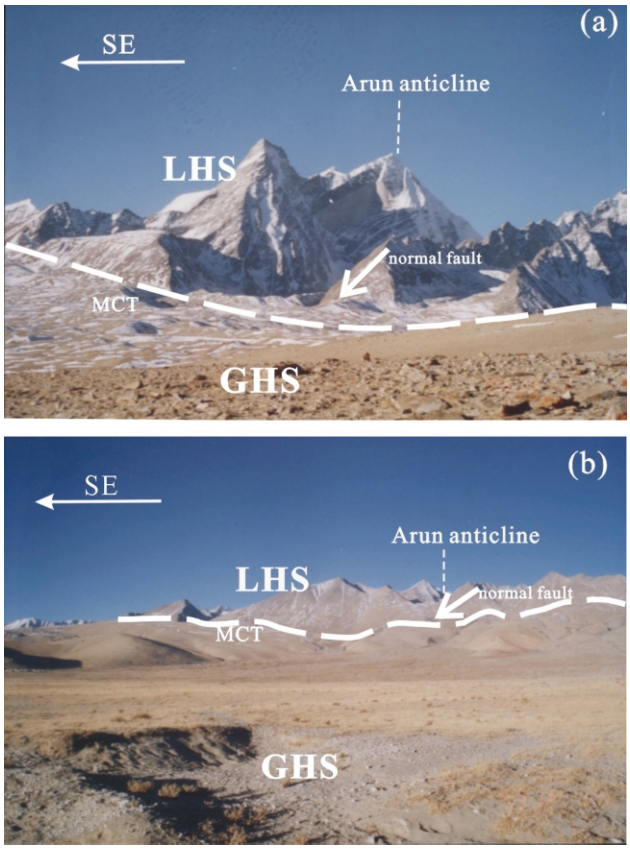

Figure 3. *a*, *b*, Field photos showing the Arun anticline, the relationship between the Greater Himalayan Sequence (GHS) and the Lesser Himalayan Sequence (LHS), and the location of the Main Central Thrust (MCT) fault. For the peak location in *a*, see figure 2*a*. The viewpoint is southwest from the Pass (see fig. 2*a*) to the southwest of Saer. See text for discussion.

km north of the Kharta, the north-northeast-trending garnet sillimanite gneisses and granites are also cut by an north-northwest-directed normal fault with a width of about 100 m, and they are juxtaposed against the North Col Formation in the hanging wall (fig. 2*a*). Two lines of evidence suggest that the contact between the North Col Formation and the garnet sillimanite gneisses and granites is a major normal fault, which is regarded as the lower STF fault: (1) it places lower-grade metamorphic rocks over higher-grade metamorphic rocks, marking a metamorphic discontinuity, and (2) rocks around the contact are strongly mylonitized. Twenty kilometers to the northwest, a northwest-directed brittle normal fault, regarded as the upper STF fault and with a width of about 100 m, separates the North Col Formation in the footwall from Ordovician to Tertiary sedimentary rocks (Wang and Zheng 1979; fig. 2*a*). In the Saer area, the upper and lower STF faults are also observed, but the thickness of the zone between these two normal faults is <2 km (fig. 2*a*).

Major Rock Formations

North Col Formation. Rocks of the North Col Formation occur below the southern Tibetan Tethyan sedimentary rocks, which were deposited in Ordovician to Tertiary times, and above the GHS (figs. 1, 2*a*), and they were initially termed the "Everest series" by Wager (1934, 1965). Comprehensive work had been done by Yin (1974), who named the rocks the "Rouqincun group," a term widely used in Chinese literature (e.g., Wei et al. 1989; Liu et al. 1990). Yin and Guo (1978) divided the group into the Yellow Band above and the North Col Formation below. Spatially, the North Col Formation occurs between Gyirong (about 85°E) and Cona (about 92°E; Liu et al. 1990; fig. 1). In the Kharta area, the North Col Formation was folded and became part of the north-northeast-trending Arun anticline (fig. 2*a*). The Yellow Band consists of pale yellow calc-silicate marble bands, which are prominent markers on Mount Qomolangma between about 8200 and 8660 m (Yin and Guo 1978). This massive marble band, approximately 200–250 m thick, contains calcite, quartz, and muscovite ± biotite. It is regarded as Ordovician in age, based on stratigraphic correlations with similar rocks in southern Tibet (Yin and Guo 1978; Burchfiel et al. 1992). The North Col Formation consists mainly of dark-colored, thin-bedded pelites and psammites. The typical mineral assemblage is albite, quartz, biotite, chlorite, and epidote ± muscovite, whereas the assemblages of scapolite + actinolite + oligoclase and garnet + biotite + muscovite + oligoclase occur at the bottom of this complex (Liu et al. 1990; Searle et al. 2003). Along the Dzakar Chu valley (fig. 2*a*), black gneisses with sillimanite + cordierite + biotite were observed to occur at the bottom of the North Col Formation (Lombardo and Rolfo 2000). Pognante and Benna (1993) have estimated 450°–550°C as the peak metamorphic temperature of the lowest North Col Formation. Compared to the GHS, where sillimanite occurs mainly as a prismatic variety, sillimanite at the bottom of the North Col Formation is fibrolite. North of Saer, this formation is also observed with peak *PT* conditions of 3.3–4.0 kbar and 470°–510°C (samples D8 and D25 of Hodges et al. 1994).

Garnet Sillimanite Gneisses. Sample 1103, a representative sample of the garnet sillimanite gneisses (for location, see fig. 2*a*; table A1, available

in the online edition or from the *Journal of Geology* office), consists of garnet, Al-silicates, quartz, plagioclase, K-feldspar, biotite, cordierite, and spinel, with minor rutile, ilmenite, apatite, zircon, and monazite. This sample exhibits a well-developed foliation, defined by the preferential orientation of sillimanite, biotite, and polycrystalline aggregates of quartz. Garnet grains, generally several millimeters in size, are euhedral to subhedral and contain abundant inclusions, such as quartz, rutile, zircon, apatite, and monazite, and are mantled by fine-grained coronas of cordierite, biotite, and plagioclase. Large grains of plagioclase and K-feldspar in the garnet sillimanite gneisses normally display exsolution textures—fine patches of alkali feldspar occurring in plagioclase or plagioclase patches in K-feldspar (Borghi et al. 2003). Under plane-polarized light, all sillimanite grains coexisting with K-feldspar, perthite, or antiperthite are prismatic, but fibrolitic mats are also discernible under crossed nicols. This feature points to sillimanite pseudomorphs formed after early kyanite. Additionally, kyanite was reported to coexist with K-feldspar in the gneisses (e.g., Wei et al. 1989; Borghi et al. 2003). These lines of petrological evidence suggest that the garnet sillimanite gneisses underwent a high-pressure (HP) granulite facies metamorphism (e.g., O'Brien and Rötzler 2003). The prismatic sillimanite aggregates were partially replaced by fine-grained intergrowths of cordierite and spinel, which also formed around garnet grains. Both newly formed assemblages reflect that the garnet sillimanite gneisses underwent further retrogression at low pressure. The determined εNd (0) value of this sample is -13.7 (table A2, available in the online edition or from the *Journal of Geology* office), as reported previously for the GHS rocks.

Granites. Granites are widespread in the garnet sillimanite gneisses of the Kharta and Saer areas, especially east and southeast of the Kharta and south of the Saer areas, where they appear at the top of the garnet sillimanite gneisses and are cut by the lower STF fault (fig. 2*a*). On the other hand, the granites are truncated by at least two sets of leucogranitic dikes. The granite plutons appear to be homogeneous in composition throughout their outcrops. Some of them have mafic lenses. Most of the granites are two-mica granites with variable amounts of muscovite and biotite as well as apatite, monazite, and zircon (Visona and Lombardo 2002).

Two representative monazite-bearing granites (samples 1303, 1504; for locations, see fig. 2*a*) were studied in detail. Sample 1303 comes from a locality that contains mafic lenses (sample 1303; see fig. 2*a*) and was taken from below the north-north-east-trending lower STF faults. Sample 1504 was collected from the so-called Tongmen granite (Wei et al. 1989; Liu et al. 1990), below the northeast-directed lower STF fault (fig. 2*a*). These rocks are homogeneous and nondeformed. The whole-rock compositions of the granites are similar to those of the sillimanite gneisses. The aluminum saturation indexes (mol% $Al_2O_3/CaO + Na_2O + K_2O$) for samples 1504 and 1303 are 1.48 and 1.10, respectively. The Rb/Sr ratios of the two granite samples are 0.5 and 7.3. The εNd values of -17.8 (table A2) are similar to values reported from the GHS (Ahmad et al. 2000; Robinson et al. 2001).

Migmatites. Migmatites, characterized by polycrystalline aggregates of quartz and feldspar, are abundant in the Arun valley north of Kharta (Borghi et al. 2003) and south of Saer. In these rocks, antiperthite coexists with perthite, quartz, and brown-red biotite. Preferential orientation of biotite defines a well-developed foliation.

Mafic Lenses. Numerous mafic lenses or boudinaged pods were observed to occur in the granites and garnet sillimanite gneisses east of Kharta and in the migmatites south of Saer (fig. 2*a*). They are interpreted as overprinted eclogites by Lombardo and Rolfo (2000) and as HP granulites by Li et al. (2003), respectively. The lenses vary in long axis length from several tens of centimeters to several meters. They are black and dense, with discernible red garnet grains several millimeters in diameter. The garnets are settled in a matrix of olive-brown amphibole and brown-red biotite and surrounded by white plagioclase rims. Under the microscope, symplectites consisting of plagioclase + clinopyroxene ± orthopyroxene (fig. 4*a*) or amphibole ± ilmenite are interpreted to have replaced primary pyroxenes. Garnets are partly replaced by coronas of plagioclase, amphibole, and ortho- and clinopyroxene. Quartz is separated from garnet by plagioclase. A few rutile grains that occur as inclusions in garnet crystals are observed to be armored by ilmenite. Late-stage olive-green amphiboles grew after clinopyroxene-plagioclase symplectites and normally include relics of the symplectites. These petrological characteristics are similar to those of strongly overprinted eclogites, such as Variscan eclogites from the Bohemian Massif (O'Brien and Vrana 1995).

Although samples of mafic lenses were collected from different locations, the whole-rock compositions are very similar. The silica content of the samples, except sample 1205, is in the range of 49–50 wt% (table A2). The Mg# values (molecular ratio of MgO/[MgO + FeO total]) and Cr, Ni, and V contents are in the ranges of 0.51–0.66 and 41–116

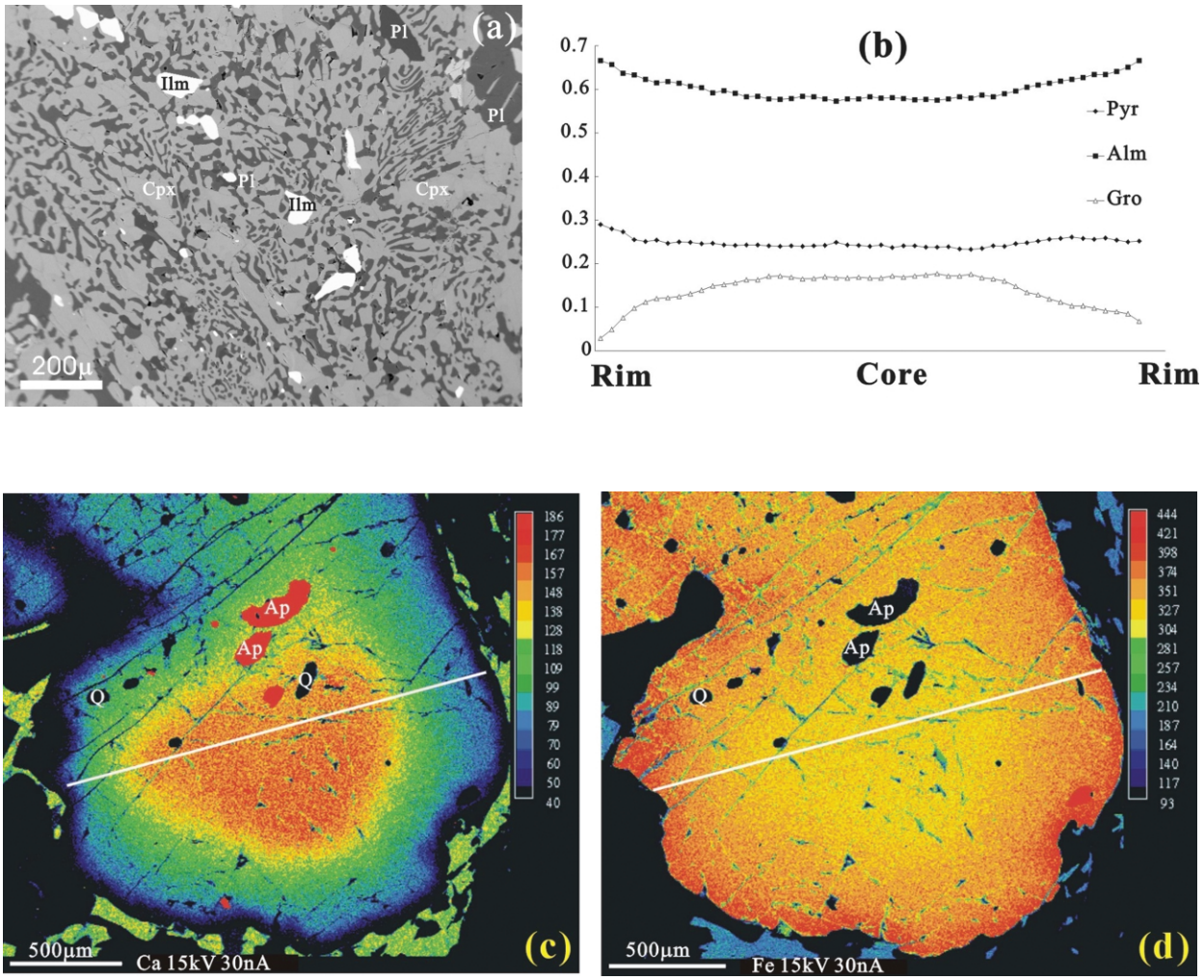

Figure 4. *a*, Backscattered electron image showing finer- and coarser-grained symplectites composed mainly of clinopyroxene and plagioclase. The symplectites are usually surrounded by coarse-grained amphibole. *b*, Compositional profile through a garnet from sample 1103. Selected data are given in table A3. *c*, *d*, X-ray maps showing compositional zoning patterns of garnet from sample 1103. White lines show the position of the compositional profile of *b*. Mineral abbreviations after Kretz (1983).

ppm, 42–76 ppm, and 474–567 ppm, respectively, suggesting that the lenses were derived from basaltic precursors. Two whole-rock isotopic analyses gave $^{143}Nd/^{144}Nd$ ratios of 0.512628 and 0.512840, corresponding to $\varepsilon Nd(0)$ values of −0.2 and 3.9. Considering their late Proterozoic formation ages (see below), the high present-day εNd values suggest that the two mafic lenses were derived from a depleted mantle source (table A2).

Amphibolite Facies Rocks. Sample 1203 taken from below the high-angle fault to the east of the Kharta valley (fig. 2) is a representative specimen of the sillimanite gneisses of the amphibolite facies rocks. This sample contains quartz, plagioclase, biotite, fibrous sillimanite, muscovite, chloritoid, and accessory garnet, zircon, apatite, and monazite. The fibrous sillimanite coexists with brown biotite, which defines the main foliation of the gneisses. Quartz and plagioclase are also elongated. Chloritoid coexists with fibrous sillimanite, suggesting that peak metamorphic *PT* conditions of the sillimanite gneisses are close to the aluminum silicate triple point (3.7 kbar and 504°C) and the kyanite and sillimanite fields. Southwest of Saer, the sillimanite gneisses from the footwall of the high-angle fault were estimated to have formed under 4.4 kbar and 550°C (sample D11 of Hodges et al. 1994). Although sample 1203 is compositionally

identical to sample 1103 (table A2), the εNd(0) value is distinctively lower (−23.4), similar to values of rocks of the LHS investigated previously (Parrish and Hodges 1996; Whittington et al. 1999; Ahmad et al. 2000; Robinson et al. 2001).

Compositions of Minerals in the Garnet Sillimanite Gneiss and Mafic Lenses: Implications for the *PT* Paths

Garnet Sillimanite Gneiss (Sample 1103). Compositional profiles and x-ray mapping have revealed that the dominant component in garnet is almandine (>57 mol%), slightly increasing from core to rim. This increase is coupled with a decrease of the grossular component (table A3, available in the online edition or from the *Journal of Geology* office; fig. 4*b*–4*d*). The compositional plateau encompassing the interior of the garnet crystal (fig. 4*b*–4*d*) suggests that the sillimanite gneisses experienced relatively high temperatures over a long period of time resulting in homogenization of the extended core region by intracrystalline diffusion (see Spear 1991). Recent work in the Kharta area by Borghi et al. (2003) and Searle et al. (2003) has revealed that the garnet sillimanite gneisses experienced temperatures ≥725°C and pressures around 8 kbar during high-temperature (HT) metamorphism. The high Fe and low Ca concentrations at the margins of the garnet crystals (fig. 4*b*–4*d*) indicate that retrograde reactions and/or diffusion took place. The *PT* conditions for this metamorphic stage were determined at about 710°C and about 3 kbar (Borghi et al. 2003), reflecting a marked decrease of pressure. Based on these data, it can be argued that the pressures of the HP event were above 8 kbar.

Mafic Lenses (Samples 1201, 1211, and 1302). The peak *PT* conditions of these lenses are virtually indeterminable because most early metamorphic minerals excluding garnet have disappeared. The composition of garnet was possibly modified by breakdown and/or diffusion under later HT metamorphism. Nevertheless, we tried to obtain information about the original composition of clinopyroxene in terms of jadeite content to estimate the (minimum) pressure of the supposed HP event. In fact, the search for inclusions of HP minerals such as omphacite in garnets from samples 1201 and 1302 was unsuccessful, but the reintegration of clinopyroxene and plagioclase in symplectites of these samples led to consistent results that pointed to the presence of early omphacite. For the reintegration method, we first determined the volumes of clinopyroxene and plagioclase in extended portions of larger symplectites, using backscattered electron images (see fig. 4*a*). The original clinopyroxene composition in terms of Na and Ca contents was calculated considering the Na_2O and CaO contents of clinopyroxene and plagioclase in the symplectites (table A4, available in the online edition or from the *Journal of Geology* office) as well as a significantly lower density of plagioclase (factor 0.8) compared with clinopyroxene. For sample 1302, the average of several reintegrations was $0.216 = X_{Na}$ (=Na/[Na + Ca]). In sample 1201, two generations of clinopyroxene-plagioclase symplectites occur, differing by the size of the lamellae of these minerals (fig. 4*a*). Nevertheless, the reintegrated X_{Na} of both symplectite generations yielded virtually the same result of 0.255. From the later value, we conclude that the original clinopyroxene was omphacite with about 25 mol% jadeite. Using the experimentally calibrated isopleths for various jadeite contents in clinopyroxene related to the equilibrium jadeite + quartz = albite by Gasparik (1985), pressures around 14 kbar result for an omphacite with 25 mol% jadeite at temperatures between 750° and 800°C. In fact, these conditions, which were similarly derived by Lombardo and Rolfo (2000), refer to minimum pressures, since quartz is abundant, but according to the unknown presence of plagioclase at HP, 14 kbar could be the true pressure during an early metamorphic event because plagioclase is also enclosed in garnet.

In spite of the somewhat uncertain *PT* estimate for the HP event, the *PT* conditions of the HT overprint could be estimated by assuming domainal equilibria were reached in small reaction volumes. Thermometers dependent on exchange reactions among the mineral pairs garnet-orthopyroxene (Harley 1984), garnet-clinopyroxene (Powell 1985), garnet-hornblende (Graham and Powell 1984), and hornblende-plagioclase (Holland and Blundy 1994) are applied here. Equilibria among garnet-plagioclase-orthopyroxene-quartz and garnet-plagioclase-clinopyroxene-quartz (Newton and Perkins 1982; Eckert et al. 1991) were used for geobarometry. According to the cited calibrations, the *PT* conditions of the overprinted metamorphic event were determined to be 7–10 kbar and 730°–810°C, again similar to estimations by Lombardo and Rolfo (2000).

New Interpretation of the Structural Framework of the Kharta Area

Two metamorphic sequences occur in the Kharta area (Visona and Lombardo 2002; Borghi et al. 2003). The structurally higher sequence consists of garnet sillimanite gneisses, migmatites, and granites, in which overprinted eclogites appear, com-

monly as lenses. The structurally lower sequence, occurring in the central part of the Arun anticline (fig. 2), consists of amphibolite facies rocks without (overprinted) eclogite lenses. The boundary between the two sequences is located about 7 km to the east of the Kharta valley (fig. 2) and southwest of Saer (fig. 2).

Integrating the *PT* conditions mentioned above, we suggest that both the garnet sillimanite gneisses and the mafic lenses (former eclogites) of the structurally higher level experienced at least a very similar *PT* evolution, as evidenced by the spatial relation of former dikes and country rocks. Both rock types underwent an early HP event, probably around 14 kbar at temperatures estimated to be in the range of 750°–800°C. If this estimate is correct, the rocks subsequently experienced a pressure release only to intermediate pressures ($P \sim 8$ kbar at 730°–810°C) to reach their present characteristics in terms of mineral compositions and fabric. Finally, low-pressure metamorphism took place at 3 kbar and 710°C. Thus, during exhumation from about 50 to 10 km, the temperatures of the rocks had only slightly decreased. The gneisses from the structurally lower sequence, however, showed *PT* conditions of 3–5 kbar and 500°–550°C. Therefore, a distinct metamorphic break occurs between the two sequences of the different structural levels. Nd isotopes (table A2) further suggest that the sequence of the structurally high level should belong to the GHS, whereas the other sequence can be related to the LHS. The boundary between these two sequences should thus be the MCT fault. Stretching lineation in the structurally lower sequence indicates that the fault was originally a north-dipping thrust. It was folded around the axis of the north-northeast-trending Arun anticline and then changed to a normal fault, which is supported by the footwall of the MCT fault with higher attitude (e.g., fig. 3*a*).

Earlier work has shown that from Zanskar in the west to Bhutan in the east, Higher Himalayan granitoids including migmatites are always bounded by the STF system (e.g., see summary in Searle et al. 2003). The majority of these granitoids exhibit peraluminous characteristics and relatively high Rb/Sr ratios (e.g., Harris and Massey 1994; Visona and Lombardo 2002; Whittington and Treloar 2002). Sample 1303, taken below the fault along the Kharta valley (fig. 2) that was regarded as the MCT (e.g., Lombardo and Rolfo 2000; Visona and Lombardo 2002; Borghi et al. 2003), also presents these geochemical characteristics, thus providing a line of evidence that the fault is a part of the STF system and not part of the MCT system, as suggested by Lombardo and Rolfo (2000). The MCT should occur about 7 km east of the Kharta valley. Based on these observations, we argue that the overprinted eclogites should belong to the GHS and not to the LHS as suggested by Lombardo and Rolfo (2000). Clearly, much work involving field mapping, petrologic studies, Nd isotopic analyses, and zircon dating is needed in the near future to address the corresponding debate.

Cathodoluminescence Investigations of Zircon for SHRIMP Analyses

Garnet Sillimanite Gneiss (Sample 1103). Cathodoluminescence (CL) investigation has revealed three different domains in the zircon grains of sample 1103 (fig. 5*a*, 5*b*). The internal domain is visible in most zircon grains and consists of an irregular or round core with medium to low CL emission. In the following, this part is referred to as core domain. Zoning patterns of these cores are not always visible. Some cores display oscillatory zoning that is truncated by later overgrowth (fig. 5*a*, 5*b*). Around the core domain, a euhedral bright overgrowth with a sector/oscillatory zoning pattern is developed, which is referred to as mantle domain. This kind of zoning pattern has been frequently observed in granulite facies or granite zircon grains (Vavra et al. 1996, 1999). K-feldspar, plagioclase, quartz, and biotite have been found as inclusions within the mantle domain. The outermost zircon domain generally forms an idiomorphic overgrowth with low CL emission, which is referred to as rim domain. The size of the rim domain varies from crystal to crystal and ranges from several to 50 μm. No inclusions were found within the rim domain.

Granites (Sample 1303). Although zircon grains in sample 1303 are smaller than those of sample 1103, the internal structure is similar based on the CL emission. Three domains can be identified in the CL images (fig. 5*c*, 5*d*) as well.

Geochronological Results

Mafic Lenses. Three representative samples (1201, 1209, and 1210) were dated using the U-Pb thermal ionization mass spectrometry (TIMS) method on zircons (table A5, available in the online edition or from the *Journal of Geology* office; fig. 6*a*). All samples yielded discordant U-Pb results, with similar $^{207}Pb/^{206}Pb$ ages that ranged from 910 to 1057 Ma. Three analyzed zircon fractions from sample 1201 define a discordia line, with upper and lower intercept ages of 971 ± 8 and 10 ± 11 Ma, respectively, and an MSWD value of 0.70. Two frac-

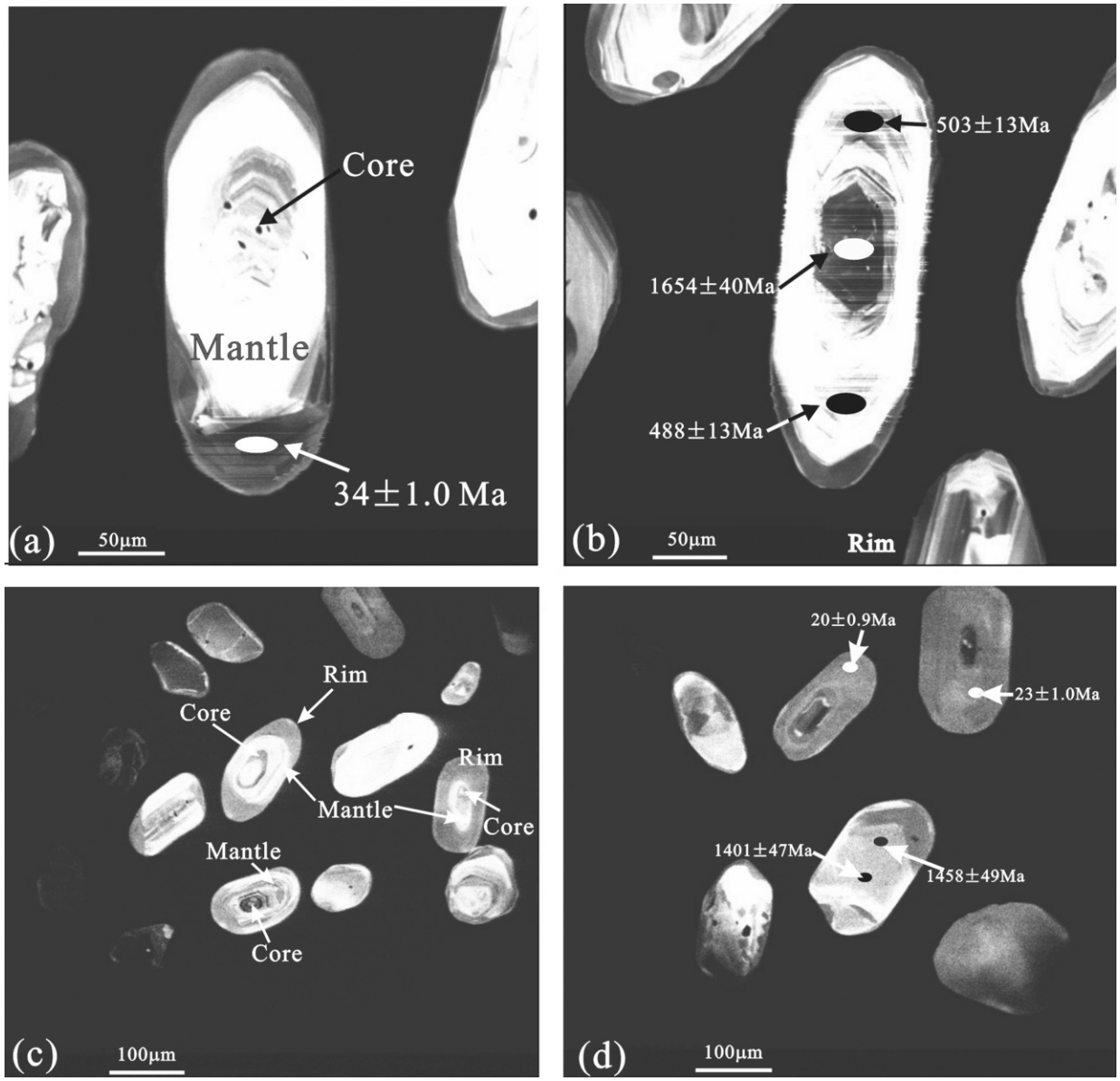

Figure 5. Cathodoluminescence images showing internal structure of zircon grains from sample 1103 (*a*, *b*) and from sample 1303 (*c*, *d*). Circles indicate SHRIMP analysis spots for which $^{206}Pb/^{238}U$ ages are given ($\pm 1\sigma$ in Ma). See text for discussion.

tions from sample 1210 gave an upper intercept age of 1122 ± 100 Ma.

Garnet Sillimanite Gneiss. Zircon grains from sample 1103 were dated using a SHRIMP in combination with CL observations. Thirty-three spots were analyzed from 11 grains, but 11 spot analyses were not used for evaluation because of larger uncertainties or mixing ages resulting from overlapping analyses on different age domains (table A6, available in the online edition or from the *Journal of Geology* office). The three different zircon domains observed during CL analyses have distinct Th/U ratios and U-Pb ages. The core domains have variable U and Th contents with high Th/U ratios (0.10–0.61) and apparent $^{206}Pb/^{238}U$ ages scattering between 546 and 1654 Ma (fig. 6*b*). The Th/U ratios of the mantle domains vary from 0.08 to 0.36. The ages obtained from this domain spread over a slightly wider range. Nevertheless, seven U-Pb analyses still define a concordia age at 493 ± 10 Ma (MSWD = 0.6; fig. 6*c*). The rim domains have very low Th/U ratios, between 0.01 and 0.04.

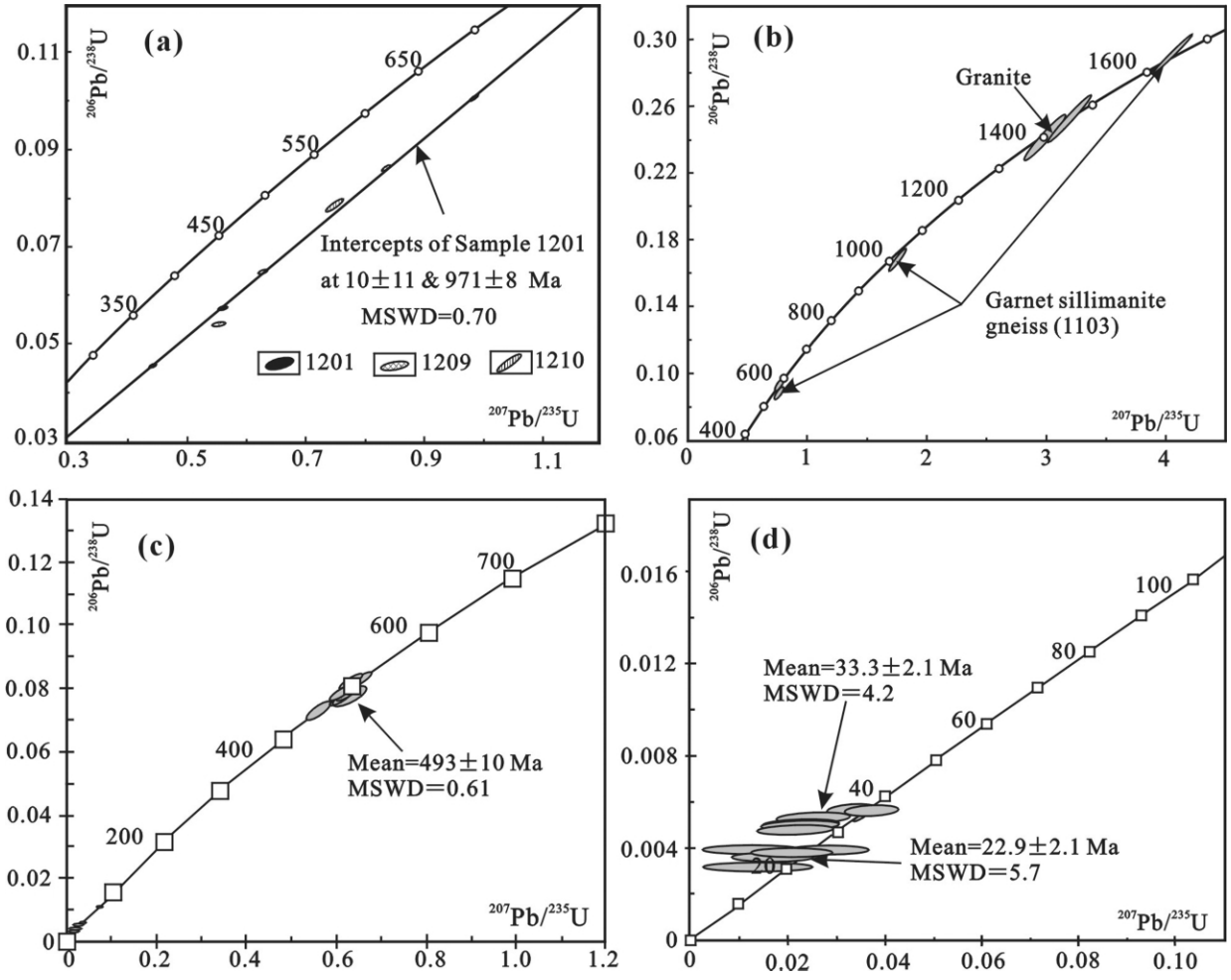

Figure 6. U-Pb concordia plots for samples from this study. *a*, Zircon U-Pb concordia plot for overprinted eclogites, showing analyses performed by the thermal ionization mass spectrometry method from three different samples: three fractions from 1201, two fractions from 1209, and two from 1210. Only three zircon fractions from sample 1201 were used for the discordia intercept calculation, using the Isoplot program (Ludwig 1999). Other fractions are shown only for comparison. Data are listed in table A5. *b–d*, Zircon U-Pb concordia plots for the core, mantle, and rim domains of zircon crystals from sample 1103. Data acquired by the SHRIMP are listed in table A6. In *b*, two analysis spots from sample 1303 are also shown for comparison. The average ages and errors with 2σ level in *c* and *d* were calculated using the Isoplot program.

Eleven analyses from the rim domain define two age groups. Apparent $^{206}Pb/^{238}U$ ages of one group range from 31 to 37 Ma, with a weighted mean age of 33 ± 2 Ma and an MSWD of 4.2 (fig. 6*d*). The apparent $^{206}Pb/^{238}U$ ages of other group, however, are between 20 and 25 Ma. The weighted mean age of this group is 23 ± 2 Ma with an MSWD of 5.7 (fig. 6*d*).

Granites. Two zircon SHRIMP analyses from the core domain of sample 1303 gave a concordia age of 1430 ± 30 Ma (table A6; fig. 6*b*). The rim part yielded an age of 20–23 Ma (table A6). These ages are similar to those of the garnet sillimanite gneiss.

Monazites from two representative samples (1504, 1303) were dated using the U-Th-Pb TIMS method. For sample 1303, one fraction (1303-4) gave a discordant result, and the U-Th-Pb ages of this fraction are slightly older, compared with the other fractions (table A7, available in the online edition or from the *Journal of Geology* office; fig. 7*a*), suggesting a minor inheritance of monazite. All other fractions of this sample are close to concordance (fig. 7*a*). Moreover, the $^{208}Pb/^{232}Th$ ages of

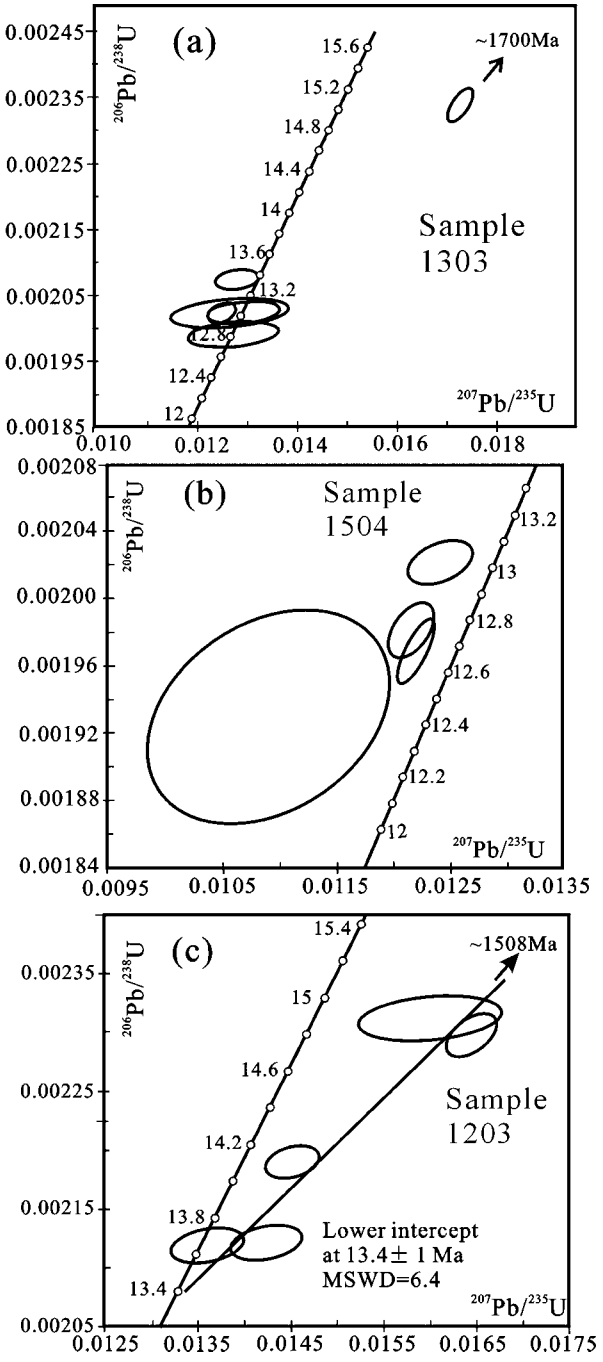

Figure 7. Monazite U-Pb concordia plots for the samples 1303 (*a*), 1504 (*b*), and 1203 (*c*). Data are listed in table A7. Processes of raw data are similar to those of zircon.

these fractions except that of fraction 1303-6, which is slightly younger, closely agree with the U-Pb ages (table A7). The mean $^{206}Pb/^{238}U$, $^{207}Pb/^{235}U$, and $^{208}Pb/^{232}Th$ ages (excluding fraction 1303-6) are 13.1 ± 0.3, 12.8 ± 0.2, and 12.7 ± 0.6 Ma, respectively. Thus, we think that monazite crystallization in sample 1303 took place around 13 Ma. Sample 1504 also includes one fraction (1504-3) that yielded normally discordant U-Pb ages. The $^{208}Pb/^{232}Th$ age of this fraction is similar to that of sample 1303-4 (table A7). This supports the inheritance interpretation. The other fractions of sample 1504 are slightly reversely discordant (table A7; fig. 7*b*). The reverse discordant effect is largely due to excess ^{206}Pb, which is derived from disequilibrium incorporation of ^{230}Th into the crystal lattice as an intermediate daughter product of the ^{238}U decay chain (Schärer 1984; Parrish 1990). In such a case, the $^{207}Pb/^{235}U$ ages are commonly regarded as the more reliable crystallization age of monazite. The $^{206}Pb/^{238}U$, $^{207}Pb/^{235}U$, and $^{208}Pb/^{232}Th$ mean ages (excluding fraction 1504-4, which has a large analytical uncertainty) are 12.7 ± 0.3, 12.4 ± 0.2, and 12.8 ± 0.3 Ma, respectively. Thus, we suggest that the crystallization of monazite in this sample occurred between 12.4 and 12.8 Ma.

Amphibolite Facies Rock. Monazites from sample 1203 were dated using the U-Th-Pb method. All fractions of sample 1203 are normally discordant in the U-Pb system (table A7; fig. 7*c*), suggesting the presence of some inherited material within the grains. A linear regression through all fractions yielded a lower intercept age of 13.4 ± 1 Ma with an MSWD of 6.4 (fig. 7*c*).

Interpretation of the U-Th-Pb Ages

The core domains of the zircon grains from the garnet sillimanite gneisses and granites gave similar ages. Zircon grains from both rock types have morphologies and zoning pattern characteristics of a detrital population. This observation is in line with the variability in U/Th ratios and Neoproterozoic ages. Thus, the detrital zircon domain reflects the age(s) of the crustal source terrain from which the precursors of the garnet sillimanite gneisses and granites were derived.

The zircon U-Pb upper intercept ages of the mafic lenses (971 ± 8 and 1122 ± 100 Ma) are interpreted as crystallization age. Taking the geochemical composition of the mafic lenses (table A2) into account, the ages are further regarded as the time of basic magmatic activity. It seems likely that the protoliths of the mafic lenses of the Kharta area are late Proterozoic basic dikes that intruded Neoproterozoic (meta)sedimentary rocks around 1 Ga. Subsequently, they were covered by late Neoproterozoic sedimentary rocks. Zircon grains in sample

1209 have morphologies that are characteristic of a detrital origin. This could be explained by their derivation from mafic tuffs. Thus, the age might not necessarily represent the age of dike intrusion. In summary, our U-Pb studies indicate that the protoliths of the GHS, including the garnet sillimanite gneisses, granites, and some mafic lenses, were formed during the Neoproterozoic.

Based on the results of Vavra et al. (1999), the zircon CL pattern and Th/U ratios could indicate that the mantle domain of the zircons formed during a HT or partial melting event. Evidence for this includes the polygonal zoning and the Th/U ratios that are similar to magmatic zircons found in intrusive rocks. As mentioned above, the inclusions in this domain are K-feldspar, plagioclase, quartz, and biotite, suggesting that the event cannot be related to HP metamorphism. Peak temperatures were too low to allow complete Pb diffusion (Lee et al. 1997), as demonstrated by the preservation of older ages in the cores. The age of the mantle domain (493 ± 10 Ma) suggests that during a late phase of the Pan-African orogeny, the Neoproterozoic (meta)sedimentary rocks and mafic dikes underwent HT metamorphism or even partial melting.

The zircon rim domain is lacking any regular zoning pattern. Moreover, it is rich in U and has a very low Th/U ratio. This is often observed in zircons from amphibolite to granulite facies rocks (e.g., Williams et al. 1996; Vavra et al. 1999; Rubatto et al. 2001), suggesting that the rocks underwent HT metamorphism during the Himalayan orogeny. The two different ages found in the garnet sillimanite gneisses (33 ± 2 and 23 ± 2 Ma) might indicate that these rocks were subjected to HT metamorphism over a protracted period of time or, alternatively, the existence of two distinct phases of zircon growth. The latter interpretation was favored by Simpson et al. (2000), who argued that the sillimanite-grade and the later cordierite-grade metamorphism of the central GHS occurred at 32.2 ± 0.4 and 22.7 ± 0.2 Ma, respectively.

The two granite samples 1504 and 1303 from the GHS yielded indistinguishable monazite U-Th-Pb ages of 12–13 Ma. However, zircon SHRIMP analyses did not give such young ages for these granites. Two analysis spots on the zircon rims gave an age of 21–22 Ma for sample 1303 (table A6), which is very close to the age of the final low-pressure metamorphic event mentioned above. During emplacement and crystallization of the granitic magmas, zircons did not develop new rims, whereas the monazites grew at the expense of apatite or other rare earth element–bearing minerals. Thus, we interpret the ages of 12–13 Ma as the time of emplacement and crystallization of granites in the Kharta area and the age of 21–22 Ma as the time of metamorphism of the premagmatic protoliths.

Monazites from the LHS (sample 1203) yielded a young U-Th-Pb age of 13.4 ± 1 Ma. U, Th, Pb, and Y mapping (fig. 8) revealed irregularly zoning patterns of monazite grains, suggesting a new growth around older inherited cores. The lower-intercept age of 13.4 ± 1 Ma is interpreted as the age of monazite overgrowth during protracted metamorphism. Field observations show that sample 1203 experienced only HT ductile shear resulting from the hot GHS overthrusting the cold LHS during the activity of the MCT fault (fig. 2). Given the lack of protective silicate minerals such as garnet, the monazites of the garnet-free sillimanite gneiss could have formed a new overgrowth zone during the HT ductile shear. Thus, the time of this new overgrowth in sample 1203 is argued to be related to the activity of the MCT fault. However, earlier studies have revealed that in the case of monazite inheritance, the lower intercept age is a maximum age estimate for the time of new monazite growth (e.g., Copeland et al. 1988; Parrish 1990). Therefore, it seems likely that the MCT was tectonically active between 12 and 13 Ma and thus was synchronous with the crystallization of the granites below the STF.

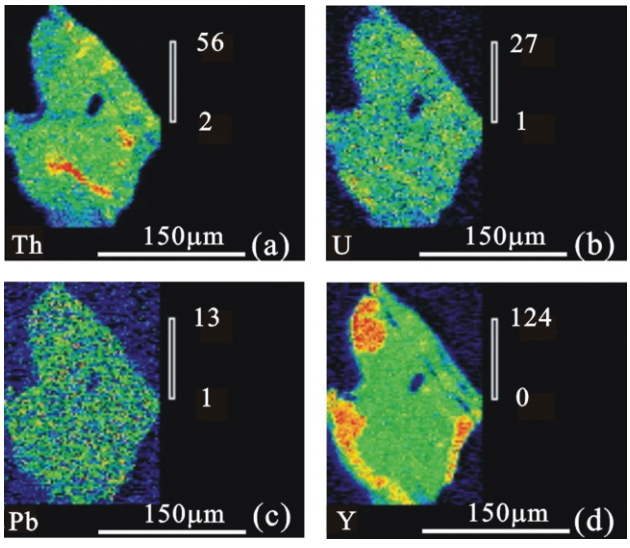

Figure 8. X-ray maps showing compositional zoning patterns of U, Th, Pb, and Y of a monazite from sample 1203.

Discussion

Although numerous geochronological studies have been performed on garnet sillimanite gneisses, which are the dominant rock type of the GHS within the central to eastern Himalayas (e.g., Simpson et al. 2000; Daniel et al. 2003; Catlos et al. 2004), it was difficult to attach these age data to the tectonometamorphic evolution of the garnet sillimanite gneisses within the Kharta area. However, zoning and mineral inclusions in zircon, which is an excellent container in which to preserve early phases that had experienced even HT and HP metamorphism, provide valuable information for solving this question.

Zircon U-Pb SHRIMP dating in combination with CL images has revealed that the garnet sillimanite gneisses and granites in the Kharta area were derived mainly from a Neoproterozoic source terrain. Zircon U-Pb TIMS dating also suggests that protoliths of some mafic lenses within the Kharta area were also late Proterozoic basic dikes. Before the collision between the Indian and Asian plates, these rocks underwent HT metamorphism at about 500 Ma to form crystalline rocks consisting of granitoids and/or paragneisses with minor mafic rocks. During collision between India and Asia, these crystalline rocks were buried beneath southern Tibet to form HP (~14 kbar = 50-km depth) granulite facies gneisses at the Oligocene, as further suggested by the zircon U-Pb SHRIMP dating. During the onset of exhumation in early Miocene times (20–23 Ma), they were transformed to low-pressure rocks marked by cordierite + spinel in gneisses. Metamorphic phase transitions might have resulted in a significant density reduction below southern Tibet in the late Oligocene to early Miocene, generating buoyancy for the uplift of southern Tibet. This, in turn, implies that southern Tibet had already achieved its higher altitude in early Miocene times.

Zircon internal CL structure, SHRIMP dating, and Nd isotopes clearly suggested that the granites and the garnet sillimanite gneisses within the Kharta area derived from the same source. Coronas of cordierite + spinel around sillimanite, biotite, and garnet in the garnet sillimanite gneisses suggest that dehydration melting of biotite, sillimanite, and garnet has taken place in a regime of adiabatic decompression through the following reaction: biotite + sillimanite + garnet = cordierite + spinel + K-feldspar + melt. This suggests that granites within the Kharta area were probably produced by dehydration melting of the GHS during exhumation. The less dense granite melts, in turn, could have contributed to further exhumation of the GHS by buoyancy. Thus, the monazite crystallization ages of these granites could constrain the exhumation age of the GHS within the Kharta area.

Structural analyses have shown that the late stage of exhumation of the GHS in the Kharta area, central Himalayas, is related to movements along the STF and MCT systems at shallow depths (fig. 2), similar to the GHS in other parts of the Himalayas (e.g., Hodges 2000; Searle et al. 2003). Our monazite dating further emphasizes that within the Kharta area at 12–13 Ma, this late exhumation of the central GHS took place. Finally, at shallow depths, the GHS and upper LHS, including the STF and the MCT within the Kharta area, underwent north-south-trending folding to form the Arun anticline after 12 Ma.

Conclusions

The central part of the north-northeast-trending Arun anticline is composed of upper LHS, which is separated from the GHS in the hanging wall by the upper MCT fault. The GHS consists of garnet sillimanite gneisses, migmatites, and granites with mafic lenses. The lower STF juxtaposes the GHS in the footwall against the North Col Formation in the hanging wall. The late stage of exhumation of the GHS within the Kharta area could be attributed to the MCT and STF systems.

The protoliths of the GHS within the Kharta area are Neoproterozoic sedimentary rocks with some mafic dikes. At about 500 Ma, this rock assemblage underwent HT metamorphism or even partial melting and was largely converted into granitoids or paragneisses with mafic inclusions.

In the Oligocene, these crystalline rocks were buried beneath southern Tibet to form HP granulite facies gneisses. In the early Miocene (20–23 Ma), phase transitions and first exhumation occurred to produce low-pressure and HT rocks below southern Tibet. In the middle Miocene (12–13 Ma), the central GHS was further exhumed from middle or even shallow crustal levels and finally underwent north-south-trending folding to form the Arun anticline at shallow crustal levels after 12 Ma. The late stage of exhumation of the GHS within the Kharta area could be attributed to the MCT and STF systems.

ACKNOWLEDGMENTS

We thank E. Reitter and Mrs. G. Bartholomä (Tübingen) for guiding sample digestion, clean-lab work and mass spectrometry, and x-ray fluorescence analysis, respectively. The aid by T. Theye (Stuttgart) for microprobe analyses and by Z. Yang (Beijing) for SHRIMP analyses and data processing is kindly acknowledged. Reviews by P. O'Brien, K. Hodges, P. Parrish, and an anonymous reviewer significantly improved earlier versions of the manuscript. We would like to thank B. Lombardo for his constructive comments, although he did not agree with some of our interpretations. This work was supported by the National Natural Science Foundation of China (grants 40272044 and 40572040), the Deutsche Forschungsgemeinschaft, Germany (grant 446 CHV 113/204/0-1), and Ministry of Land and Resources, China (grant 200101020405).

REFERENCES CITED

Ahmad, T.; Harris, N.; Bickle, M.; Chapman, H.; Bunbury J.; and Prince, C. 2000. Isotopic constraints on the structural relationships between the Lesser Himalayan Series and the High Himalayan Crystalline Series, Garhwal Himalaya. Geol. Soc. Am. Bull. 112: 467–477.

Black, L. P.; Kamo, S. L.; Allen, C. M.; Aleinikoff, J. N.; Davis, D. W.; Korsch, R. J.; and Foudoulis, C. 2003. TEMORA 1: a new zircon standard for Phanerozoic U-Pb geochronology. Chem. Geol. 200:155–170.

Borghi, A.; Castelli, D.; Lombardo, B.; and Visona D. 2003. Thermal and baric evolution of garnet granulites from the Kharta region of S Tibet, E Himalaya. Eur. J. Mineral. 15:401–418.

Burchfiel, B. C.; Chen, Z. L.; Hodges, K. V.; Liu, Y. P.; Royden, L. H.; Deng, C. G.; and Xu, J. 1992. The south Tibetan detachment system, Himalayan orogen: extension contemporaneous with and parallel to shortening in a collisional mountain belt. Geol. Soc. Am. Spec. Pap. 269:1–41.

Catlos, E. J.; Dubey, C. S.; Harrison, T. M.; and Edwards, M. A. 2004. Late Miocene movement within the Himalayan Main Central Thrust shear zone, Sikkim, north-east India. J. Metamorph. Geol. 22:207–226.

Chen, F.; Hegner, E.; and Todt, W. 2000. Zircon ages and Nd isotopic and chemical compositions of orthogneisses from the Black Forest, Germany: evidence for a Cambrian magmatic arc. Int. J. Earth Sci. 88:791–802.

Chinese Academy of Sciences. 1962. Scientific exploration of the Mount Jolmo Lungma (1959–1960). Beijing, Science, 291 p. (in Chinese).

Chinese Academy of Sciences. 1974. Scientific exploration of the Mount Jolmo Lungma (1966–1968). Beijing, Science, 299 p. (in Chinese).

Chinese Academy of Sciences. 1979. Scientific exploration of the Mount Jolmo Lungma (1975). Beijing, Science, 221 p. (in Chinese).

Compston, W.; Williams, I. S.; Kirschvink, J. L.; Zhang, Z.; and Ma, G. 1992. Zircon U-Pb ages for the Early Cambrian timescale. J. Geol. Soc. Lond. 149:171–184.

Copeland, P.; Parrish, R. R.; and Harrison, T. M. 1988. Identification of inherited radiogenic Pb in monazite and its implications for U-Pb systematics. Nature 333: 760–763.

Daniel, C. G.; Hollister, L. S.; Parrish, R. R.; and Grujic, D. 2003. Exhumation of the main central thrust from lower crustal depths, eastern Bhutan Himalaya. J. Metamorph. Geol. 21:317–334.

Droop, G. T. R. 1987. A general equation for estimating Fe^{3+} microprobe analyses, using stoichiometric criteria. Miner. Mag. 51:431–435.

Eckert, O. J.; Newton, R. C.; and Kleppa, O. J. 1991. The H of reaction and recalibration of garnet-pyroxene-plagioclase-quartz geobarometers in the CMAS system by solution calorimetry. Am. Mineral. 76:148–160.

Gasparik, T. 1985. Experimentally determined compositions of diopside-jadeite pyroxene in equilibrium with albite and quartz at 1200–1350°C and 15–34 kbar. Geochim. Cosmochim. Acta 49:865–870.

Graham, C. M., and Powell, R. 1984. A garnet-hornblende geothermometer: calibration, testing, and application to the Pelona schist, southern California. J. Metamorph. Geol. 2:13–31.

Harley, S. L. 1984. An experimental study of the partitioning of Fe and Mg between garnet and orthopyroxene. Contrib. Mineral. Petrol. 86:359–373.

Harris, N. B. W., and Massey, J. 1994. Decompression and anatexis of Himalayan metapelite. Tectonics 13:1537–1546.

Hodges, K. V. 2000. Tectonics of the Himalaya and southern Tibet from two perspectives. Geol. Soc. Am. Bull. 112:324–350.

Hodges, K. V.; Hames, W. E.; Olszewski, W.; Burchfiel, B. C.; Royden, L. H.; and Chen. Z. 1994. Thermobarometric and $^{40}Ar/^{39}Ar$ geochronologic constraints on Eohimalayan metamorphism in the Dinggye area, southern Tibet. Contrib. Mineral. Petrol. 117:151–163.

Hodges, K. V.; Parrish, R. R.; and Searle, M. P. 1996. Tectonic evolution of the central Annapurna Range, Nepalese Himalaya. Tectonics 15:1264–1291.

Holland, T. J. B., and Blundy, J. D. 1994. Non-ideal interactions in calcic amphiboles and their bearing on amphibole-plagioclase thermometry. Contrib. Mineral. Petrol. 116:433–447.

Kaneko, Y.; Katayama, I.; Yamamoto, H.; Misawa, K.; Ishikawa, M.; Rehman, H. U.; Kausar, A.; and Shiraishi, K. 2003. Timing of Himalayan ultrahigh-pressure metamorphism: sinking rate and subduction angle of

the Indian continental crust beneath Asia. J. Metamorph. Geol. 21:589–599.
Kretz, R. 1983. Symbols for rock-forming mineral. Am. Mineral. 68:277–279.
Lee, J. K. W.; Williams, I. S.; and Ellis, D. J. 1997. Pb, U and Th diffusion in natural zircon. Nature 390:159–161.
Leech, M. L.; Singh, S.; Jain, A. K.; Klemperer, S. L.; and Manickavasagam, R. M. 2005. The onset of India-Asia continental collision: early, steep subduction required by the timing of UHP metamorphism in the western Himalaya. Earth Planet. Sci. Lett. 234:83–97.
Li, D.; Liao, Q.; Yuan, Y.; Wan, Y.; Liu, D.; Zhang, X.; Yi, S.; Cao, S.; and Xie, D. 2003. SHRIMP U-Pb zircon geochronology of granulites at Rimana (Southern Tibet) in the central segment of Himalayan Orogen. Chin. Sci. Bull. 48:2647–2650.
Liu, G.; Jin, C.; Wang, F.; Wang, S.; Wang, B.; Xu, R.; and Ding, X. 1990. Metamorphic and igneous rocks in Xizang (Tibet). People's Republic of China Ministry of Geology and Mineral Resources Geological Memoirs, Series 3, no. 11. Beijing, Geological, 380 p. (in Chinese with English abstract).
Lombardo, B., and Rolfo, F. 2000. Two contrasting eclogite types in the Himalaya: implications for the Himalayan orogeny. J. Geodyn. 30:37–60.
Ludwig, K. R. 1988. Pbdat for MS-DOS: a computer program for IBM-PC compatibles for processesing raw Pb-U-Th isotope data. U.S. Geol. Surv. Open File Rep. 88-542, p. 1–37.
———. 1999. Isoplot/Ex, version 2.06: a geochronological tool-kit for Microsoft Excel. Berkeley Geochronology Center Spec. Publ. 1a, p. 1–49.
Massonne, H.-J., and O'Brien, P. J. 2003. The Bohemian Massif and the NW Himalaya. *In* Carswell, D. A., and Compagnoni, R., eds. Ultrahigh pressure metamorphism. EMU Notes Mineral. 5:145–187.
Newton, R. C., and Perkins, D. 1982. Thermodynamic calibration of geobarometers based on the assemblages garnet-plagioclase-orthopyroxene (clinopyroxene)-quartz. Am. Mineral. 67:203–222.
O'Brien, P. J., and Rötzler, J. 2003. High-pressure granulites: formation, recovery of peak conditions and implications for tectonics. J. Metamorph. Geol. 21:3–20.
O'Brien, P. J., and Vrana, S. 1995. Eclogites with a short-lived granulite facies overprint in the Moldanubian Zone, Czech Republic: petrology, geochemistry and diffusion modelling of garnet zoning. Geol. Rundsch. 84:473–488.
O'Brien, P. J.; Zotov, N.; Law, R.; Khan, M.; Ahmed, M.; and Qasim, J. M. 2001. Coesite in Himalayan eclogite and implications for models of India-Asia collision. Geology 29:435–438.
Parrish, R. R. 1990. U-Pb dating of monazite and its application to geological problems. Can. J. Earth Sci. 27: 1431–1450.
Parrish, R. R., and Hodges, K. V. 1996. Isotopic constraints on the age and provenance of the Lesser and Greater Himalayan sequences, Nepalese Himalaya. Geol. Soc. Am. Bull. 108:904–911.
Pognante, U., and Benna, P. 1993. Metamorphic zonation, migmatization, and leucogranites along the Everest transect (eastern Nepal and Tibet): record of an exhumation history. *In* Treloar, P. J., and Searle, M. P., eds. Himalayan tectonics. Geol. Soc. Lond. Spec. Publ. 74:323–340.
Powell, R. 1985. Regression diagnostics and robust regression in geothermometer/geobarometer calibration: the garnet-clinopyroxene thermometer revisited. J. Metamorph. Geol. 3:327–340.
Robinson, D. M.; DeCelles, G.; Patchett, P. J.; and Garzione, C. N. 2001. The kinematic history of the Nepalese Himalaya interpreted from Nd isotopes. Earth Planet. Sci. Lett. 192:507–521.
Rubatto, D.; Williams, I. S.; and Buick, I. S. 2001. Zircon and monazite response to prograde metamorphism in the Reynolds Range, central Australia. Contrib. Mineral. Petrol. 140:458–468.
Sachan, H. K.; Mukherjee, B. K.; Ogasawara, Y.; Maruyama, S.; Ishida, H.; Muko, A.; and Yoshioka, N. 2004. Discovery of coesite from Indus Suture Zone (ISZ), Ladakh, India: evidence for deep subduction. Eur. J. Mineral. 16:345–366.
Schärer, U. 1984. The effect of initial ^{230}Th disequilibration on U-Pb ages: the Makalu case. Earth Planet. Sci. Lett. 67:191–204.
Searle, M. P.; Simpson, R. L.; Law, R. D.; Parrish, R. R.; and Waters, D. J. 2003. The structural geometry, metamorphic and magmatic evolution of the Everest massif, high Himalaya of Nepal–south Tibet. J. Geol. Soc. Lond. 160:345–366.
Simpson, R. L.; Parrish, R. R.; Searle, M. K.; and Waters, D. J. 2000. Two episodes of monazite crystallization during metamorphism and crustal melting in the Everest region of the Nepalese Himalaya. Geology 28: 403–406.
Spear, F. S. 1991. On the interpretation of peak metamorphic temperatures in light of garnet diffusion during cooling. J. Metamorph. Geol. 9:379–388.
Stacey, J. S., and Kramers, J. D. 1975. Approximation of terrestrial lead isotope evolution by a two-stage model. Earth Planet. Sci. Lett. 26:207–221.
Vavra, G.; Gebauer, D.; Schmidt, R.; and Compston, W. 1996. Multiple zircon growth and recrystallization during polyphase Late Carboniferous to Triassic metamorphism in granulites of the Ivrea Zone (southern Alps): an ion microbprobe (SHRIMP) study. Contrib. Mineral. Petrol. 122:337–358.
Vavra, G.; Schmidt, R.; and Gebauer, D. 1999. Internal morphology, habit and U-Th-Pb microanalysis of amphibolite-to-granulite facies zircons: geochronology of the Ivrea Zone (southern Alps). Contrib. Mineral. Petrol. 134:380–404.
Visona, D., and Lombardo, B. 2002. Two-mica and tourmaline leucogranites from the Everest-Makalu region (Nepal-Tibet): Himalayan leucogranite genesis by isobaric heating? Lithos 62:125–150.
Wager, L. R. 1934. A review of the geology and some new observations. *In* Ruttledge, H., ed. Everest 1933. London, Hodder & Stoughton, p. 312–336.

———. 1965. Injected granite sheets of the Rongbuk valley and the north face of Mount Everest. *In* D. N. Wadia commemorative volume. Kolkata, India Mining, Geology and Metallurgy Institute, p. 358–379.

Wang, Y., and Zheng, X. 1979. Imbricate structure in the northern slope of Jolmo Lungmo and discussion on the uplift of the Himalaya. *In* Chinese Academy of Sciences, eds. Scientific exploration of Jolmo Lungma (1975). Beijing, Science, p. 199–221 (in Chinese).

Wei, G.; Shi, S.; Mao, Y.; Zhang, B.; and Shun, S. 1989. Geological structure and metamorphism of Precambrian system in Himalayan region. Chengdu, Chengdu University of Science and Technology Press, 176 p. (in Chinese with English abstract).

Whittington, A. G.; Foster, G.; Harris, N.; Vance, D.; and Ayres, M. 1999. Lithostratigraphic correlations in the western Himalaya: an isotopic approach. Geology 27: 585–588.

Whittington, A. G., and Treloar, P. J. 2002. Crustal anatexis and its relation to the exhumation of collisional orogenic belts, with particular reference to the Himalaya. Miner. Mag. 66:53–91.

Williams, I. S.; Buick, I. S.; and Cartwright, I. 1996. An extended episode of early Mesoproterozoic metamorphic fluid flow in the Reynolds Range, central Australia. J. Metamorph. Geol. 14:29–47.

Yin, J. 1974. Stratigraphy of the Mount Jolmo Lungma area (Cambrian to Ordovician). *In* Chinese Academy of Sciences, eds. Scientific exploration of the Mount Jolmo Lungma (1966–1968). Beijing, Science, p. 4–23 (in Chinese).

Yin, J., and Guo, S. 1978. Stratigraphy of the Mount Jolmo Lungma and its north slope. Sci. Sin. 21:629–644.